Journal of Materials Chemistry A

Accepted Manuscript

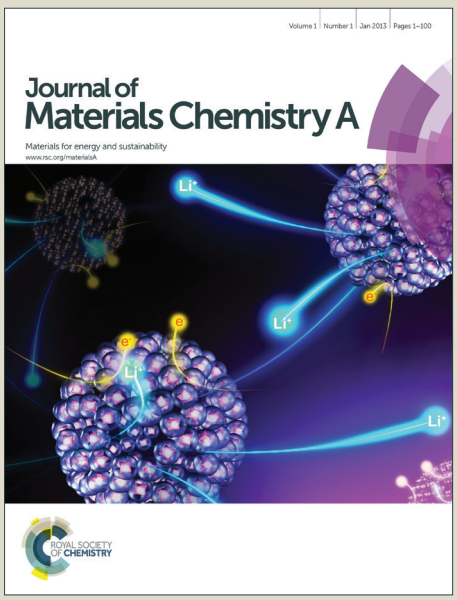

ROYAL SOCIETY OF CHEMISTRY

www.rsc.org/materialsA

Journal Name

ARTICLE

Rapid and Discriminative Detection of Nitro Aromatic Compounds with High Sensitivity by Two Zinc MOFs Synthesized through Temperature-Modulated Method

Received 00th January 20xx,
Accepted 00th January 20xx

DOI: 10.1039/x0xx00000x

www.rsc.org/

Xiu-Yan Wan[ab], Fei-Long Jiang[a], Cai-Ping Liu[a], Kang Zhou[a], Lian Chen[a]*, Yan-Li Gai[a], Yan Yang[ab] and Mao-Chun Hong[a]*

Two 3D MOFs (**1**-**2**) have been solvothermally synthesized by introducing a π-electron conjugated fluorescent aromatic polycarboxylate ligand under the modulation of reaction temperature. Intriguingly, complex **2** shows an unusual fluorescence thermochromism. Upon decreasing the temperature, the emission bands exhibit different variation behaviors which result in the dramatically changes of the emission color. The fluorescence of **1** and **2** dispersed in DMF (N,N-dimethylformamide) can be selectively and sensitively quenched by nitro aromatic compounds (NACs) with fast response time of just 10 s, indicating that **1** and **2** are potential real-time response candidates for detecting NACs. More interestingly, when DNP (2,4-dinitrophenol) and PNA (p-nitroaniline) are introduced, the distinctive fluorescent signals, which can discriminate them from other NACs, are observed, making **1** and **2** the rare materials to distinguish different NACs.

Introduction

The rapid and selective detection of chemical explosives is urgently required for the consideration of homeland security, military applications and humanitarian implications.[1] Since nitro aromatic compounds (NACs), such as 2,4-dinitrophenol (DNP), p-nitrosophenol (PNP), p-nitroaniline (PNA), p-nitrosotoluene (PNT) and nitrobenzene (NB), are principal components of explosives, it is very crucial to detect NACs in liquid/vapor phase for tracing buried and underwater explosives. At present, the detection methods mainly rely on trained canines and sophisticated instruments.[2] However, the present instrumental techniques usually suffer from the disadvantage of high cost on instruments and portability issues. Therefore, chemical sensors, which are much more inexpensive and easy to portable, with excellent operability, short response time and high sensitivity are in high demand for applications in detection of NACs.[3]

Most NACs can act as good fluorescent quenchers due to the presence of electron-deficient -NO_2 groups, which makes sensors based on fluorescence quenching to be the most effective tools for detection of NACs.[4] Fluorescence-based metal-organic frameworks (MOFs), with the existence of π-electron rich aromatic organic ligands, have proven to exhibit high selectivity towards NACs.[5] The delocalized π-electrons can increase the electrostatic interactions between polymers and electron deficient nitro aromatic molecules with the result of fluorescent quenching. Since Li et al. reported the first fluorescence-based MOF which can detect trace nitro aromatic explosives in the vapor phase,[6] increasing attentions have been paid to fluorescent MOFs with π-electron rich aromatic organic ligands for the detection of NACs in recent years.[7] For example, Chang and Bu et al. have synthesized a 3D Cd-based MOF which could be used as an efficient fluorescence sensor for nitrobenzene in solution or vapor state.[5g] Ghosh's group reported a 3D fluorescent metal–organic framework exhibited selective detection of TNP (2,4,6-trinitrophenol), even in the presence of other nitro compounds in both aqueous and organic solution.[7d] Chen and Qian's group made use of a luminescent nanoscale MOF for the straightforward and highly sensitive sensing of the nitro aromatic explosives.[7g] Although much effort has been devoted to the exploration of fluorescence-based MOFs as chemical sensors toward NACs, developing quick and highly selective sensors for NACs, especially real-time monitors of NACs with fast response time, is still a huge challenge.[8] On the other hand, it is equally important to mention that even though lots of work has been done on detecting NACs from other small molecules, few examples involve discriminative detection of different NACs.[9] In fact, for the practical applications, selective detection of different kinds of NACs is much more critical. Thus, the investigation of discriminative detection for different NACs, which is still in its infancy, remains an imperative issue that presses for exploration.

[a] *Key Laboratory of Design and Assembly of Functional Nanostructures,Fujian Institute of Research on the Structure of Matter, Chinese Academy of Sciences, Fuzhou, 350002, China,E-mail: hmc@fjirsm.ac.cn; cl@fjirsm.ac.cn*
[b] *Graduate School of the Chinese Academy of Sciences, Beijing, 100049, China.*
Electronic Supplementary Information (ESI) available: Additional crystallographic, PXRD, TG-MS, IR and fluorescence data, computational methods, theoretical calculated results. CCDC 1054076-1054077. For ESI and crystallographic data in CIF or other electronic format see DOI: 10.1039/x0xx00000x

As we all know, the properties of MOFs largely depend on their structures, so the primary issue is to obtain MOFs with preferred structures. However, how to precisely control the structures of MOFs on the molecular level is still a severe challenge. It has become evident that the self-assembly of MOFs depends on many factors, such as metal ions, organic ligands, reaction temperatures, pH values, reagent ratios, solvents and so on.[10] Though there is no convergence with regard to these influence factors, reaction temperature has proven to have remarkable influences on the formations and structures of MOFs.[11] It is generally accepted that organic ligands, especially carboxylate ligands, may adopt different coordination modes under different temperatures.[12] Thereby, it is hopeful that diverse fascinating structures could be obtained by adopting carboxylate ligands through temperature-modulated method. In this work, two three-dimensional (3D) fluorescent MOFs, $\{[Me_2NH_2][Zn_4(H_2L)(L)]\cdot 2H_2O\cdot 2DMF\}_n$ (**1**) and $\{[Zn_4(\mu_3\text{-}OH)_2(L)(H_2O)_2]\cdot 2DMF\}_n$ (**2**), have been solvothermally synthesized by introducing the π-electron conjugated fluorescent aromatic polycarboxylate ligand [1,1';4',1"]terphenyl-3,5,2',5',3",5"-hexacarboxylic acid (H_6L) under the modulation of reaction temperature. The structures of these two complexes are analysed and compared. Fluorescent properties are investigated at room temperature and cryogenic temperatures to track their responses to temperature. The detection experiment results show that **1** and **2** can not only detect trace amounts of NACs from other aromatic compounds with high sensitivity and rapid response time, but also can distinguish DNP and PNA from the other NACs.

Experimental Section

Materials and methods

All chemicals and solvents used were purchased from commercial sources and used without further purification. All the solvents used were analytically pure, except for the DMF used in detection experiments, which was spectrum pure. The C, H, and N microanalyses were determined using an ElementarVario MICRO elemental analyzer. IR spectra were recorded in 400-4000 cm^{-1} region by means of PerkinElmer SpectrumOne FT-IR spectrometer with KBr pellets (5 mg of sample in 500 mg of KBr). The power X-ray diffraction (PXRD) data was collected on Cu-Kα radiation equipped with RIGAKU DMAX 2500 diffractometer at room temperature. Thermal gravimetric analyzer-mass spectrometry (TG-MS) was performed on a Netzsch STA 449C instrument and a Balzers MID instrument heated from room temperature to 1000 °C under nitrogen atmosphere. Fluorescent spectra at different temperatures in solid state were investigated on FLS920 with 450W xenon light. Fluorescent spectra for detection experiments were taken on the Horiba Fluorolog-3 instrument with 450W xenon light.

Syntheses of $\{[Me_2NH_2]_2[Zn_4(H_2L)(L)]\cdot 2H_2O\cdot 2DMF\}_n$ (1). A mixture of $Zn(NO_3)_2\cdot 6H_2O$ (297 mg, 1 mmol), H_6L (99 mg, 0.2 mmol), DMF (5 mL), H_2O (5 mL) and HNO_3 (0.2 mL) was sealed in a 25 mL Teflon-lined stainless steel container. When the container was sealed and heated at 120 °C for 3 days then cooled at a rate of 4 °C·h^{-1} to 30 °C, colourless crystals of complex **1** were obtained with the yield of 65% based on H_6L. Anal. Calcd (%) for $C_{58}H_{52}N_4O_{28}Zn_4$ (Mr = 1514.68): C: 45.99%, H: 3.46%, N: 3.70%; Found: C: 46.08%, H: 3.42%, N: 3.75%; IR spectra (KBr, cm^{-1}): 3132 (w), 1679 (s), 1633 (s), 1579 (s), 1433 (s), 1371 (s), 1263 (m), 1205 (m), 1085 (w), 1010 (w), 916 (w), 769 (s), 725 (m), 663 (m), 588 (w), 449 (m).

Syntheses of $\{[Zn_4(\mu_3\text{-}OH)_2(L)(H_2O)_2]\cdot 2DMF\}_n$ (2). The synthetic method employed in **2** is similar to the method used in **1**, except that the reaction temperature is adjusted to 150 °C. Colourless crystals of **2** were obtained with the yield of 57% based on H_6L. Anal. Calcd (%) for $C_{30}H_{32}N_2O_{20}Zn_4$ (Mr = 1002.21): C: 35.95%, H: 3.22%, N: 2.80%; Found: C: 36.02%, H: 3.25%, N: 2.87%. IR spectra (KBr, cm^{-1}): 3585 (m), 1633 (s), 1398 (s), 1355 (s), 1099 (w), 920 (w), 777 (m), 588 (w), 457 (w).

X-ray crystallography

Single-crystal X-ray diffraction data were collected on a SuperNova diffractometer equipped with a Multilayers mirror Cu-Kα radiation (λ = 1.5418 Å) by using a ω scan mode. The crystal structures were solved by direct methods and refined by full-matrix least-squares on F^2 using SHELXTL package[13]. Anisotropic refinement was applied to non-hydrogen atoms. Hydrogen atoms from aromatic carbon were generated geometrically, while those on the water molecules could not be determined. All free solvent molecules in **1** and **2** can be determined by single-crystal X-ray diffraction data, except one disordered isolated water molecule in the channel of **1**. The existence of the free water molecules of **1** and the final chemical formulas of **1**-**2** are confirmed by TG-MS (Fig. S3 and S4) and elemental analysis data. The CCDC numbers are 1054076-1054077 for **1**-**2**. Crystal data and refinement details of **1** and **2** are given in Table S3.

Results and Discussion

Synthesis and characterization

The solvothermal method under high pressure and at moderate temperature (100-200 °C) has proved to be very effective for the preparation of MOFs with better crystallinity.[14] The synthetic procedures of complexes **1** and **2** are illustrated in Scheme 1. As the other reaction conditions, including the metal salt, ligand, metal-ligand ratio, solvent, and reaction time, in their synthetic procedures are totally same, reaction temperature here could be viewed as the exclusive factor which affects the final structures.

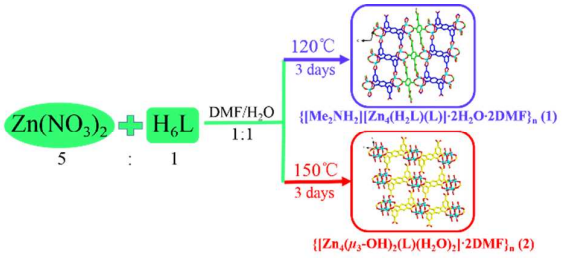

Scheme 1 Schematic drawing of the synthetic processes.

The measured PXRD patterns of the two complexes are shown in Fig. S1. They are well matched to the patterns simulated from the single-crystal data, indicating the high purities of the two samples.

Complexes **1** and **2** are stable in the air (Fig. S2) and insoluble in water and common organic solvents at room temperature. TG-MS results reveal that complex **1** exhibits really high thermal stability, whose framework is stable up to 400 °C (Fig. S3). Complex **2** exhibits relatively lower thermal stability, and its framework collapses at about 180 °C (Fig. S4), which might be attributed to the participation of water molecules in the coordination environments of metal ions.

Description of crystal structures

Structure of 1. X-ray single-crystal analysis reveals that complex **1** features a typical pillar-supporting 3D framework. The framework of complex **1** is constructed from asymmetric paddle-wheel $[Zn_2(COO)_3]$ clusters (Fig. 1a circle) and two different coordination modes of the ligand (Fig. S7a and S7b). These two different coordination modes of the ligand exhibit different degrees of deprotonation, of which, one is completely deprotonated and the other is partially deprotonated with two protons left. As shown in Fig. 1a, the layer structure in **1** is composed of two kinds of infinite ladder-like chains (chain A and chain B), which have different rungs originated from different coordination modes of the ligands. The neighbouring chains are connected with each other by sharing handrails formed by the $[Zn_2(COO)_3]$ clusters. Due to the characteristic of multiple coordination points of both the metal clusters and ligands, the layers are further pillared into a 3D framework (Fig. 1b). The framework of **1** is negatively charged, in which, the dimethylamine cations act as counterions to balance the charges and stabilize the structure. There exists one kind of rectangular channels along *a* axis with the dimension of 6.291 × 9.500 $Å^2$ (Fig. 1c), which is occupied by dimethylamine cations, DMF molecules and water molecules. Calculated by the PLATON program, the solvent accessible volume is about 33.6%.

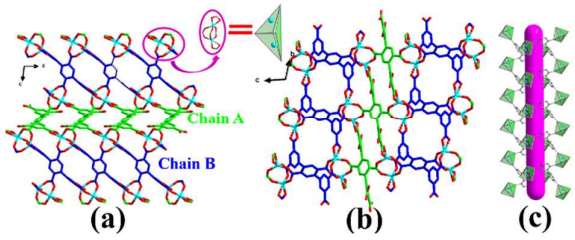

Fig. 1 (a) The layer structure in **1** (circle: asymmetric paddle-wheel $[Zn_2(COO)_3]$ cluster). (b) The 3D framework of **1**viewed along *a* axis; (c) Schematic representation of the channel in **1**.

Structure of 2. The structure of complex **2** also adopts pillar supporting construction process and is constructed from metal clusters and organic ligands with only one coordination mode which is completely deprotonated (Fig. S7c). In **2**, one deprotonating water molecule, -OH, acts asa μ_3-bridge to coordinate with three Zn ions. Two –OH μ_3-bridges linked with each other by sharing two Zn ions, giving rise to a relatively uncommon chair-like tetranuclear $[Zn_4(\mu_3\text{-}OH)_2(COO)_2]$ cluster (Fig. 2a circle). If we cut the organic ligand in **2** into three parts based on the three benzene rings, we can find out that the metal clusters and the middle parts of the ligand connected with each other extending to a 1D infinite chain (Fig. 2a). The 1D chains are linked together through the conjugating of the three parts of the ligand, resulting in a 2D layer structure (Fig. 2b). These layers are pillared to form the 3D framework owing to the nature of multiple coordination points of the metal clusters and ligands (Fig. 2c). Different from **1**, the framework of **2** is electrically neutral. Complex **2** shows one kind of rectangular channel along *a* axis with the dimension of 6.434 × 8.430 $Å^2$ (Fig. 2d), a slightly smaller than those in **1**. About 31.1% solvent-accessible volume is estimated by PLATON software. The guest DMF and water molecules are encapsulated in the voids.

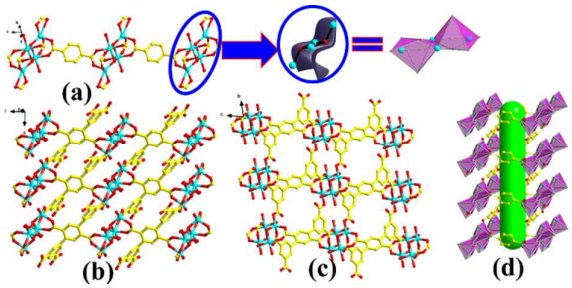

Fig. 2 (a) The 1D infinite chain formed by chair-like tetranuclear $[Zn_4(\mu_3\text{-}OH)_2(COO)_2]$ clusters (circle) and the middle parts of ligand; (b) The 2D layer structure in **2**; (c) The 3D framework of **2** viewed along *a* axis; (d) Schematic representation of the channel in **2**.

Effect of the temperature on the structures of complexes

Based on the discussions above, it can be speculated that the variation of reaction temperature during the synthetic processes results in different structures, which are mainly originated from diverse metal clusters and different coordination modes of the ligands. How the temperature affects final structures is discussed as bellow.[15]

Firstly, the structures of **1** and **2** are constructed from different metal clusters. The cluster in complex **1** is an asymmetric paddle-wheel $[Zn_2(COO)_3]$ cluster, while in complex **2** it is a relatively uncommon chair-like tetranuclear $[Zn_4(\mu_3\text{-}OH)_2(COO)_2]$ cluster. The cluster in **2** is more complicated than that in **1**. We assume that the increase of temperature can not only result in more complicated coordination environments of metal ions, but also is beneficial for the water molecules to deprotonate and coordinate with metal ions. Thus, higher temperature may induce the formation of more complicated metal clusters.

Secondly, there are different coordination modes of ligand in **1** and **2**. Complex **2** are synthesized under relative higher temperature, and the ligands in **2** are completely deprotonate. Half of the ligands in **1**, which is obtained at lower temperature, are partly deprotonated. It is conjectured that higher temperature is beneficial for the in situ hydrolysis of DMF which will give rise to dimethylamine cations. The existence of dimethylamine cations and abovementioned deprotonated water molecules will make the ligand to lose more protons. Therefore,

different reaction temperatures will result in different coordination modes of ligand which are the important components of different frameworks.

In summary, the reaction temperature mainly influences the formation of the different metal clusters and coordination modes of the ligand, which further result in the differences of the final structures such as the charges of frameworks, the guest molecules, sizes of channels. Thus, the reaction temperature can be considered as a structure-directing factor, playing a crucial role in adjusting the resultant structures.

Fluorescent properties

MOFs with d^{10} metal centers have been investigated for fluorescent properties owing to their various applications as photoactive materials.[16] The fluorescent properties of **1** and **2**, as well as the free H_6L ligand, have been investigated in the solid state at room temperature and cryogenic temperature. At room temperature, the spectrum of **1** (Fig. 3a) displays an intense emission band centered at 410 nm with excitation maximum at 340 nm. It can be attributed to the intraligand charge transfer because of the similar peak position and profile compared with the free ligand (Fig. S8)[17], which is consistent with the evaluated densities of states (DOS) for complex **1** (Fig. S9). Different from **1**, the spectrum of **2** at room temperature shows a dual emission: the high-energy (HE) emission peaked at 388 nm assigned to the intraligand charge transfer, and the low-energy emission (LE) centered at 505 nm originated from ligand-to-metal charge transfer (LMCT).[18] The speculated photoluminescent mechanisms are confirmed by the evaluated DOS for **2** (Fig. S9). For complex **2**, When the temperature decreases to 10 K, the spectrum of **1** (Fig. 3b) shows no obvious change. As for **2**, the changes are obvious and interesting: the intensity of the emission peak at HE band exhibits slightly enhancement, while the intensity of the shoulder peak at LE band enhances quite a lot which is almost ten times the intensity of the peak observed at HE band. The different intensity changes of two peaks indicate that the complex **2** may have thermochromic phenomena. The dramatic intensity increment of emission peak at LE band under cryogenic temperature is probably caused by the significant reduction of the radiationless decay rate in the process of $\pi\rightarrow\pi^*$ transition of ligand.[19]

To further investigate fluorescence thermochromic behavior of complex **2**, the fluorescent spectra are recorded during 10 K to 290 K to track its response to temperature. As illustrated in Fig. 4a, the intensity of the emission peak at 388 nm enhances slowly with the dropping of the temperature, while the intensity of emission band at 500 nm increases quite rapidly. The CIE (Commission Inter-national de L'Eclairage) 1931 chromaticity coordinates of **2** are calculated and marked as shown in Fig. 4b. The CIE chromaticity diagram shows that the emission color of **2** is located at blue-green area at room temperature. Along with the temperature decreases to 230 K, the emission color is shifted to green region relatively fast. When the temperature keeps dropping below 230 K, the emission color is stuck in green region with very slightly changes, especially during 90-10 K, in which, the chromaticity coordinates are exactly the same (Table S1). The above results about emissions in response to temperatures reveals that complex **2** may be a potential candidate for applications in temperature-sensing devices.

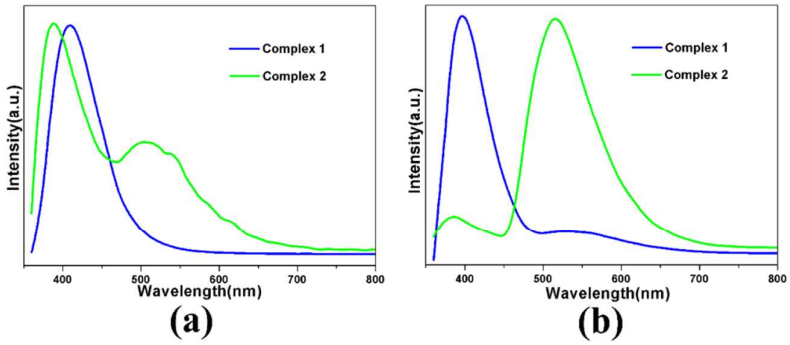

Fig. 3 Fluorescent spectra of complexes at different temperatures: (a) room temperature (290 K); (b) cryogenic temperature (10 K).

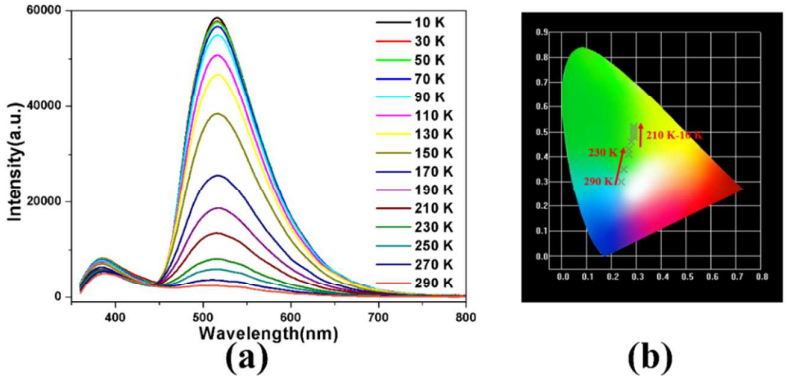

Fig. 4 (a) Fluorescent spectra of **2** at different temperatures. (b) CIE-1931 chromaticity diagram of **2** at different temperatures.

Detection of nitro aromatic compounds (NACs)

The selective fluorescence detection properties of **1** and **2** for small molecules were examined in DMF emulsions. 5 mg grinding samples of **1** and **2** were suspended in 5 mL DMF to form emulsions, respectively. Then the fluorescent experiments of these emulsions with addition of 50 μL aromatic solvents were taken under room temperature. Different from those in the solid state, the fluorescent spectra of **1** and **2** in DMF at room temperature are similar. Complex **2** exhibits only one asymmetric broad emission band peaked at 398 nm with no obvious shoulder peak (Fig. 5). This difference might be caused by the dispersion characteristic of complex in solvent, which is confirmed by the fluorescent spectra of **2** suspended in ten different solvents (Fig. S10). Since the sensing behaviors of **1** and **2** are similar, here we chose **2** as the example to describe their sensing properties.

As depicted in Fig. 5a, the fluorescent intensities largely depend on the added aromatic molecules. The intensity is stronger than the DMF emulsions when benzene is introduced while the intensities partially decreases in different degrees when methylbenzene, ethylbenzene and isopropylbenze are added. The maximum change in the intensity is no more than 44% when the above four aromatic solvents are introduced. But in the particular situation of nitrobenzene (NB), completely quenching behavior is observed. The results suggest that **2** can be employed as the chemical sensor for NB. The relationship of fluorescent intensity with the concentration of NB is investigated in more detail to examine the sensing sensitivity of **2** towards NB (Fig. 5b). The fluorescent intensity is significant quenched with quenching effiency (QE) ≈ 50% at 24 ppm and completely quenched (QE ≈ 97%) at 120 ppm. Here, the QE (%)is defined as $(1-I/I_0) \times 100\%$, in which, I_0 and I are the maximum fluorescent intensities before and after the addition of analytes, respectively. These results show that **2** exhibits high sensitivity to nitrobenzene. Furthermore, additional four nitro-substituted aromatic compounds, 2,4-Dinitrophenol (DNP), p-nitrosophenol (PNP), p-nitroaniline (PNA) and p-nitrosotoluene (PNT), were chosen to systematically investigate the sensing properties for NACs. As shown in Fig. 6, all the four NACs can also be well detected by **2** with very high sensitivity. For example, the emission intensity is significant quenched (QE ≈ 50%) when only 3 ppm DNP introduced and completely quenched (QE ≈ 97%) at 22 ppm. The high sensitivities of all the four NACs, as well as NB, are higher than most of recent reported MOFs probes for NACs.[20] The concentrations of different NACs when significant and completely quenching occurs are represented in Table 1. It is particularly worth mentioning that all of the fluorescent measurements were performed within only 10 s, which represents the fastest response time of MOF-based fluorescent probes.[21]

Although lots of MOFs sensing NACs with high selectivity and sensitivity have been demonstrated and reported, there are still some limitations for them to be applied in practice. One critical limitation is that the majority of reported fluorescent MOF sensors are based solely on fluorescent quenching, it's difficult to distinguish different NACs with just fluorescent intensity changes.[22] Remarkably, upon careful examination of the fluorescent spectra, we find two intriguing characteristics that can be used to distinguish different NACs. Firstly, when DNP is introduced to the DMF emulsions, a new emission band graduallyappears at ~480 nm (LE band). Along with the increasing of concentration, the intensity of LE band decreases quite slowly compared to the intensity of original peak at ~398 nm (HE band). The intensity of LE band begins to be stronger than the HE band from theconcentration of 10 ppm. The emergence and increase of the LE band suggested the formation of exciplex (excited complex) by the interaction of DNP and MOFs in the excited states. [9a, 23]The appearance of relatively stronger LE band can be the signature to distinguish DNP from other NACs. Secondly, for PNA, the spectra are obviously red-shift compared to pure DMF emulsions. The red-shift becomes higher along with the increase of the PNA concentration. For example, when significant quenching occurrs, the spectrum is red-shifted about 40 nm. The observed red-shift in the fluorescent spectra may be due to the formation of L-NAC complexes. In DMF solvent, the nitro aromatic molecules might be attached to the ligand to form L-NAC complexes through the π-π weak interactions (Fig. S11 and Table S4). Compared with the ligand, L-PNA exhibit obviously smaller energy gap (Table S5), which results in the photon-induced transition energy decreases and the fluorescent spectrum shifts to more red. Therefore, **2** can also be used to distinguish PNA from different nitro aromatic molecules. Compared with most of previous work about MOFs-based fluorescent probes for NACs, complex **2** can not only detect NACs with high sensitivity and rapid response time, but also distinguish DNP and PNA from other NACs.

According to related literatures,[24] the reason for quenching behaviors in NACs could be attributed to the electron transfer from the electron-donating frameworks to the highly electron-deficient NACs adhered to the surface of the frameworks. This theory could also be used to explain the quenching behavior here. As illurated in Fig. S9, S11-S12 and Table S5, the energies for LUMO orbits of NACs and L-NAC complexes are lower than that of conduction bands (CB) of ligands. Upon excitation, electrons are transferred from the valence band (VB) to the LUMOs of the NACs, leading to a quenching effect. [21b] As illustrated in Table 1, the order of sensitivity is DNP > PNA > PNP > NB > PNT. The trend is consistent with the trend of electron deficiency, which could prove the abovementioned theory for fluorescent quenching. The quenching efficiency of the analytes can be quantitatively explained by the Stem-Volmer (SV) equation.As shown in Fig. S13, the SV plots of **2** for analytes exhibitnonlinear curves (positive curvatures). The plots are nearly linear at low concentrations and deviate from linearity at higher concentrations. This nonlinear plots of **2** may result from both dynamitic (collisional) and static quenching.[25] The fluorescent data of **1** for detection experiments are represented in Fig. S14-S17 and Table S2, which are similar to those of **2**. The PXRD patterns show that **1** and **2** can remain stable after detection experiments (Fig. S18-S19).

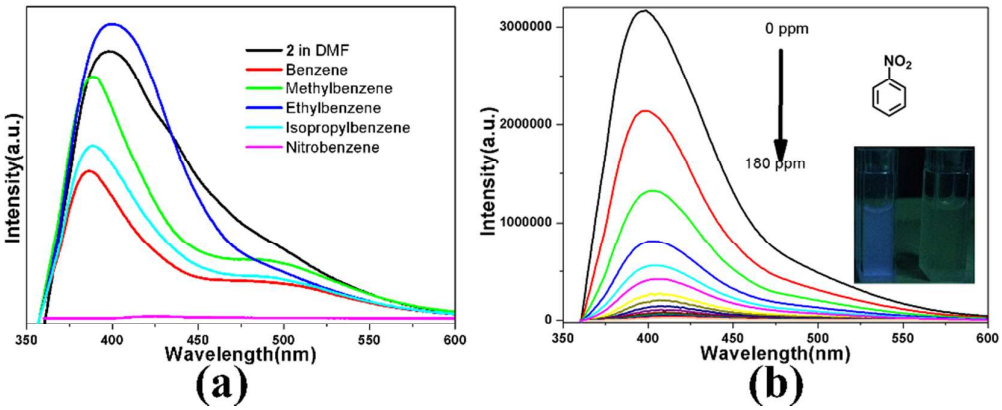

Fig. 5 (a) The fluorescent spectra of **2**suspended in DMF with the addition of aromatic solvents. (b) Fluorescent spectra of **2**suspendedin DMF with NB under λ_{ex}=350 nm.

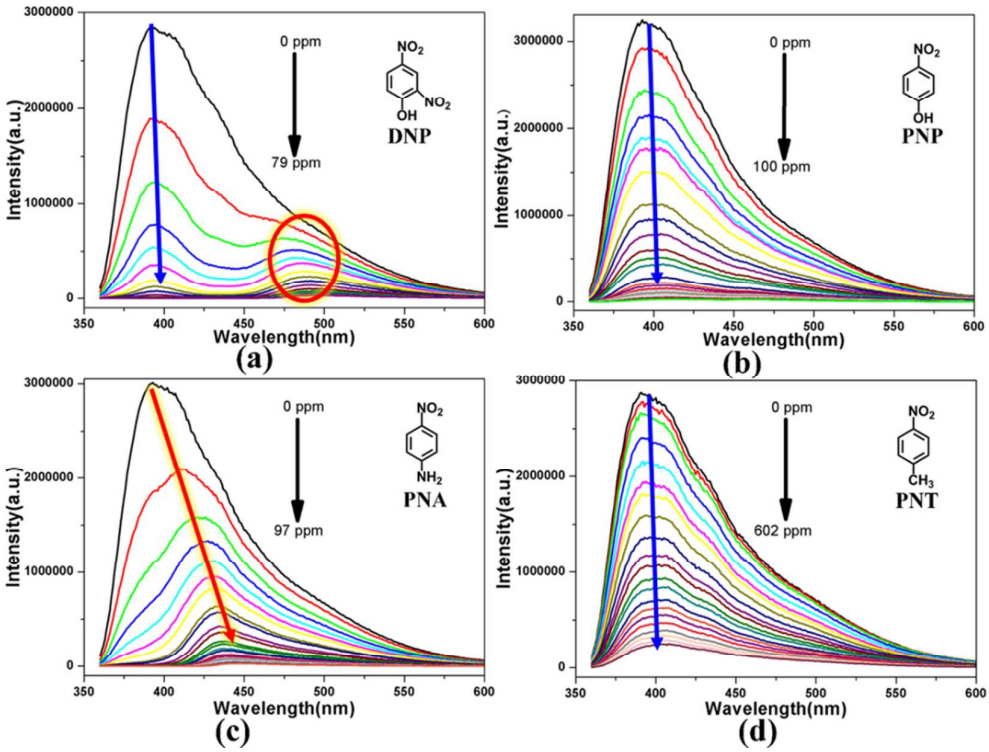

Fig. 6 Fluorescent spectra of **2**suspendedin DMF with different NACs concentrations under λ_{ex}=350 nm: (a) DNP; (b) PNP; (c) PNA; (d) PNT.

Conclusions

Two zinc MOFs were synthesized by varying the reaction temperatures on the basis of same starting materials. The structural analyses indicate that reaction temperature plays an important role in the formation of the metal clusters and coordination modes of ligand, which further leads to the difference of final structures. The fluorescent spectra and CIE-1931 chromaticity diagram at different temperatures reveal that complex **2** has color-tunable fluorescent property in response to temperature. The fluorescent detection studies reveal that **1** and **2** can serve as highly selectivity and sensitivity fluorescent probes for detecting NACs. In particular, they can detect NACs with a fast response time of just 10s, which makes them promising materials for real-time monitoring of nitro explosives. Furthermore, when DNP and PNA are introduced, the observed unique fluorescent signatures may be employed to distinguish them from other nitro aromatic molecules.

Table 1 The concentrations of different NACs when significant and completely quenching occurred for **2**.

	Significant Quenching (QE = 50%)	Completely Quenching (QE = 97%)
DNP	3 ppm	22 ppm
PNA	4 ppm	44 ppm
PNP	8 ppm	58 ppm
NB	24 ppm	120 ppm
PNT	100 ppm	602 ppm (QE = 91%)

Acknowledgements

We are thankful for financial support from the 973 Program (2013CB933200), National Natural Foundation of China (21390392, 21131006), and The CAS/SAFEA International Partnership Program for Creative Research Teams.

Notes and references

1 (a) M. E. Germain, M. J. Knapp, *Chem. Soc. Rev.* 2009, **38**, 2543-2555; (b) Y. S. Xue, Y. He, L. Zhou, F. J. Chen, Xu, Y.; H. B. Du, X. Z. You, B. L. Chen, *J. Mater. Chem. A* 2013, **1**, 4525-4530; (c) S. J. Toal, W. C. Trogler, *J. Mater. Chem.* 2006, **16**, 2871-2883; (d) Z. Q. Shi, Z. J. Guo, H. G. Zheng, *Chem. Commun.* 2015, **39**, 8300-8303.

2 (a) A. W. Czarnik, *Nature* 1998, **394**, 417-418; (b) D. S. Moore, *Rev. Sci. Instru.* 2004, **75**, 2499-2512.

3 (a) N. Niamnont, N. Kimpitak, K. Wongravee, P. Rashatasakhon, K. K. Baldridge, J. S. Siegel, M. Sukwattanasinitt, *Chem. Commun.* 2013, **8**, 780-782; (b) S. Shanmugaraju, P. S. Mukherjee, *Chem-Eur. J.* 2015, **18**, 6656-6666; (c) H. Sohn, M. J. Sailor, D. Magde, W. C. Trogler, *J. Am. Chem. Soc.* 2003, **125**, 3821-3830; (d) W. B. Wu, S. H. Ye, G. Yu, Y. Q. Liu, J. G. Qin, Z. Li, *Macromol. Rapid Comm.* 2011, **33**, 164-171; (e) S. Ghosh, S. Mukherjee, *Organometallics* 2008, **27**, 316-319; (f) J. Z. Liu, Y. C. Zhong, P. Lu, Y. N. Hong, J. W. Y. Lam, M. Faisal, Y. Yu, K. S. Wong, B. Z. Tang, *Polymer Chem.* 2010, **1**, 426-439; (g) N. N. Sang, C. X. Zhan, D. P. Cao, *J. Mater. Chem. A* 2015, **3**, 92–96.

4 (a) X. Z. Song, S. Y. Song, S. N. Zhao, Z. M. Hao, M. Zhu, X. Meng, L. L. Wu, H. J. Zhang, *Adv. Func. Mater.* 2014, **24**, 4034-4041; (b) S. Barman, J. A. Garg, O. Blacque, K. Venkatesan, H. Berke, *Chem. Commun.* 2012, **90**, 11127-11129; (c) Y. Salinas, R. Martinez-Manez, M. D. Marcos, F. Sancenon, A. M. Costero, M. Parra, S. Gil, *Chem. Soc. Rev.* 2012, **3**, 1261-1296; (d) Z. F. An, C. Zheng, R. F. Chen, J. Yin, J. J. Xiao, H. F. Shi, Y. Tao, Y. Qian,W. Huang, *Chem-Eur. J.* 2012, **49**, 15655-15661; (e) P. Anzenbacher, Jr., L. Mosca, M. A. Palacios, G. V. Zyryanov, P. Koutnik, *Chem-Eur. J.* 2012, **40**, 12712-12718; (f) J. W. Ye, X. X. Wang, R. F. Bogale, L. M. Zhao, H. Cheng, W. T. Gong, J. Z. Zhao, G. L. Ning, *Sensors Actua. B-Chem.* 2015, **210**, 566-573; (g) M. Jurcic, W. J. Peveler, C. N. Savory, D. O. Scanlon, A. J. Kenyone, I. P. Parkin, *J. Mater. Chem. A* 2015, **3**, 6351–6359.

5 (a) S. S. Nagarkar, A. V. Desai, S. K. Ghosh, *Chem. Commun.* 2014, **50**, 8915-8918; (b) B. Gole, A. K. Bar, P. S. Mukherjee, *Chem. Commun.* 2011, **44**, 12137-12139; (c) B. Gole, A. K. Bar, P. S. Mukherjee, *Chem-Eur. J.* 2014, **41**, 13321-13336; (d) S. Pramanik, Z. Hu, X. Zhang, C. Zheng, S. Kelly, J. Li, *Chem-Eur. J.* 2013, **47**, 15964-15971; (e) T. K. Kim, J. H. Lee, D. Moon, H. R. Moon, *Inorg. Chem.* 2013, **2**, 589-595; (f) D. Tian, Y. Li, R. Y. Chen, Z. Chang, G. Y. Wang, X. H. Bu, *J. Mater. Chem. A*2014, **5**, 1465-1470; (g) D. K. Singha, S. Bhattachary, P. Majee, S. K. Mondal, M. Kumara, P. Mahata, *J. Mater. Chem. A* 2014, **2**, 20908–20915.

6 A. J. Lan, K. H. Li, H. H. Wu, D. H. Olson, T. J. Emge, W. Ki, M. Hong, J. Li, *Angew. Chem. Int. Ed.* 2009, **13**, 2334-2338.

7 (a) Z. C. Hu, B. J. Deibert, J. Li, *Chem. Soc. Rev.* 2014, **43**, 5815-5840. (b) A. J. Lan, K. H. Li, H. H. Wu, L. Z. Kong, N. Nijem, D. H. Olson, T. J. Emge, Y. J. Chabal, D. C. Langreth, M. C. Hong, J. Li, *Inorg. Chem.* 2009, **15**, 7165-7173; (c) H. Wang, W. Yang, Z. M. Sun, *Chem-Asian J.* 2013, **5**, 982-989; (d) S. S. Nagarkar, B. Joarder, A. K. Chaudhari, S. Mukherjee, S. K. Ghosh, *Angew. Chem. Int. Ed.* 2013, **10**, 2881-2885; (e) C. Y. Zhang, Y. K. Che, Z. X. Zhang, X. M. Yang, L. Zang, *Chem. Commun.* 2011, **8**, 2336-2338; (f) F. Y. Yi, W. Yang, Z. M. Sun, *J. Mater. Chem.* 2012, **43**, 23201-23209; (g) H. Xu, F. Liu, Y. J. Cui, B. L. Chen, G. D. Qian, *Chem. Commun.* 2011, **11**, 3153-3155; (h) Z. J. Zhang, S. C. Xiang, X. T. Rao, Q. Zheng, F. R. Fronczek, G. D. Qian, B. L. Chen, *Chem. Commun.* 2010, **38**, 7205-7207.

8 (a) D. X. Ma, B. Y. Li, X. J. Zhou, Q. Zhou, K. Liu, G. Zeng, G. H. Li, Z. Shi, S. H. Feng, *Chem. Commun.* 2013, **49**, 8964-8966; (b) B. Joarder, A. V. Desai, P. Samanta, S. Mukherjee, S. K. Ghosh, *Chem-Eur. J.,* 2015, **21**, 965-969; (c) S. R. Zhang, D. Y. Du, J. S. Qin, S. L. Li, W. W. He, Y. Q. Lan, Z. M. Su, *Inorg. Chem.* 2014, **53**, 8105-8113; (d) J. D. Xiao, L. G. Qiu, F. Ke, Y. P. Yuan, G. S. Xu, Y. M. Wang, X. Jiang, *J. Mater. Chem. A* 2013, **1**, 8745-87582.

9 (a) S. R. Zhang, D. Y. Du, J. S. Qin, S. J. Bao, S. L. Li, W. W. He, Y. Q. Lan, P. Shen, Z. M. Su, *Chem.-Eur. J.* 2014, **20**, 3589-3594; (b) K. S. Asha, K. Bhattacharyya, S. Mandal, *J. Mater. Chem. C* 2014, **2**, 10073-10081.

10 (a) N. Stock, S. Biswas, *Chem. Rev.* 2012, **112**, 933–969; (b) Y. B. Zhang, W. X. Zhang, F. Y. Feng, J. P. Zhang, X. M. Chen, *Angew. Chem. Int. Ed.* 2009, **48**, 5287-5290; (c) C. Wang, T. Zhang, W. B. Lin, *Chem. Rev.* 2012, **2**, 1084-1104; (d) H. C. Zhou, J. R. Long, O. M. Yaghi, *Chem. Rev.* 2012, **2**, 673-674; (e) Y. Q. Tian, Y. M. Zhao, Z. X. Chen, G. N. Zhang, L. H. Weng, D. Y. Zhao, *Chem.-Eur. J.* 2007, **15**, 4146-4154; (f) M. Eddaoudi, J. Kim, N. Rosi, D. Vodak, J.,Wachter, M. O'Keeffe, O. M. Yaghi, *Science* 2002, **295**, 469-472.

11 (a) W. W. Sun, C. Y. Tian, X. H. Jing, Y. Q. Wang,E. Q. Gao, *Chem. Commun.* 2009, **31**, 4741-4743; (b) P. Shen, W. W. He, D. Y. Du, H. L. Jiang, S. L. Li, Z. L. Lang, Z. M. Su, Q. Fu,Y. Q. Lan, *Chem. Sci.* 2014, **4**, 1368-1374; (c) L. Luo, K. Chen, Q. Liu, Y. Lu, T.-a. Okamura, G. C. Lv, Y. Zhao, W. Y. Sun, *Cryst. Growth Des.* 2013, **13**, 2312-2321; (d) Y. B. Dong, Y. Y. Jiang, J. Li, J. P. Ma, F. L. Liu, B. Tang, R. Q. Huang, S. R. Batten, *J. Am. Chem. Soc.* 2007, **129**, 4520-4521.

12 (a) F. Ragon, H. Chevreau, T. Devic, C. Serre, P. Horcajada, *Chem.-Eur. J.* 2015, **19**, 7135-7143; (b) Y. X. Sun, W. Y. Sun, *Chinese Chem. Lett.* 2014, **25**, 823-828; (c) J. Cepeda, S. Pérez-Yáñez, *Chem.-Eur. J.* 2014, **20**, 3221-3234; (d) A.

Tissot, L. Rechignat, A. Bousseksou, M. L. Boillot, *J. Mater. Chem.* 2012, **8**, 3411-3419.
13 G. M. Sheldrick, SHELXS-97, Programs for X-ray Crystal Structure Solution; University of Göttingen: Germany, 1997.
14 (a) J. J. Zhang, L. Wojtas, R. W. Larsen, M. Eddaoudi, M. J. Zaworotko, *J. Am. Chem. Soc.* 2009, **131**, 17040–17041; (b) G. H. Wang, Y. Q. Lei, N. Wang, R. L. He, H. Q. Jia, N. H. Hu, J. W. Xu, *Cryst. Growth Des.* 2010, **2**, 534-540; (c) J. Niu, J. Hua, X. Ma, J. Wang, *CrystEngComm* 2012, **11**, 4060-4067.
15 (a) H. Wang, S. J. Liu, D. Tian, J. M. Jia, T. L. Hu, *Cryst. Growth Des.* 2012, **12**, 3263-3270; (b) X. X. Lu, Y. H. Luo, Y. Xu, H. Zhang, *CrystEngComm*2015, **7**, 1631-1636.
16 (a) B. L. Chen, Y. Yang, F. Zapata, G. N. Lin, G. D. Qian, E. B. Lobkovsky, *Adv. Mater.* 2007, **19**, 1693-1696; (b) B. L. Chen, L. Wang, Y. Xiao, F. R. Fronczek, M. Xue, Y. Cui, G. Qian, *Angew. Chem. Int. Ed.* 2009, **3**, 500-503; (c) J. S. Qin, S. J. Bao, P. Li, W. Xie, D. Y. Du, L. Zhao, Y. Q. Lan, Z. M. Su, *Chem-Asian J.* 2014, **3**, 749-753; (d) X. H. Jin, J. K. Sun, L. X. Cai, J. Zhang, *Chem. Commun.* 2011, **9**, 2667-2669.
17 X. Y. Wan, F. L. Jiang, L. Chen, J. Pan, K. Zhou, K. Z. Su, J. D. Pang, G. X. Lyu, M. C. Hong, *CrystEngComm*2015, **20**, 3829-3837.
18 (a) S. L. Zheng, X. M. Chen, *Aust. J. Chem.* 2004, **57**, 703-712; (b) M. D. Allendorf, C. A. Bauer, R. K. Bhakta, R. J. Houk, *Chem. Soc. Rev.* 2009, **5**, 1330-1352; (c) V. W.-W. Yam, K. K.-W. Lo, *Chem. Soci. Rev.* 1999, **28**, 323-334; (d) X. Y. Wan, F. L. Jiang, L. Chen, M. Y. Wu, M. J. Zhang, J. Pan, K. Z. Su, Y. Yang, M. C. Hong, *Cryst. Growth Des.* 2015, **3**, 1481-1491.
19 (a) X. C.. Shan, F. L. Jiang, D. Q. Yuan, H. B. Zhang, M. Y. Wu, L. Chen, J. Wei, S. Q. Zhang, J. Pan, M. C. Hong, *Chem. Sci.* 2013, **4**, 1484-1489; (b) Q. L. Zhu, T. L. Sheng, C. H. Tan, S. M. Hu, R. B. Fu, X. T. Wu, *Inorg. Chem.* 2011, **16**, 7618-7624.
20 (a) G. Y. Wang, C. Song, D. M. Kong, W. J. Ruan, Z. Chang, Y. Li, *J. Mater. Chem. A* 2014, **7**, 2213-2220; (b) Y. N. Wang, P. Zhang, J. H. Yu, J. Q. Xu, *Dalton Trans.*2015, **4**, 1655-1663; (c) Z. F. Wu, B. Tan, M. L. Feng, A. J. Lan, X. Y. Huang, *J. Mater. Chem. A* 2014, **18**, 6426-6431; (d) E. L. Zhou, P. Huang, C. Qin, K. Z. Shao, Z. M. Su, *J. Mater. Chem. A* 2015, **14**, 7224-7228.
21 (a) L. E. Kreno, K. Leong, O. K. Farha, M. Allendorf, R. P. Van Duyne, J. T. Hupp, *Chem. Rev.* 2012, **2**, 1105-1125; (b) S. Pramanik, C. Zheng, X. Zhang, T. J. Emge, J. Li, *J. Am. Chem. Soc.* 2011, **12**, 4153-4155; (c) P. F. Shi, H. C. Hu, Z. Y. Zhang, G. Xiong, B. Zhao, *Chem. Commun.* 2015, **19**, 3985-3988; (d) C. Y. Sun, X. L. Wang, C. Qin, J. L. Jin, Z. M. Su, P. Huang, K. Z. Shao, *Chem.-Eur. J.* 2013, **11**, 3639-3645; (e) X. Zhao, X. H. Bu, T. Wu, S. T. Zheng, L. Wang, P. Y. Feng, *Nat. Commun.* 2013, **4**, 2344-2352.
22 (a) W. J. Li, J. LV, S. Y. Gao, Q. H. Li, R. Cao, *J. Mater. Chem. A* 2014, **45**, 19473-19478; (b) M. H. Lim, S. J. Lippard, *Acc. Chem. Res.* 2007, **40**, 40-51.
23 (a) A. Bencini, E. Berni, A. Bianchi, P. Fornasari, C. Giorgi, J. C. Lima, C. Lodeiro, M. J. Melo, J. S. de Melo, A. J. Parola, F. Pina, J. Pina, B. Valtancoli, *Dalton Trans.* 2004, **14**, 2180–2187; (b) K. Iwai, K. Yamamoto, F. Takemura, M. Furue, S. Nozakura, *Macromolecules* 1985, **18**, 1021–1025; (c) S. Tazuke, *Makromol. Chem. Phys.* 1985, **14**, 145–159; (d) H. Loenhardt, A.Weller, *Ber. Bunsenges. Phys. Chem.* 1963, **67**, 791-795; (e) Birks J B. *Photophysics of Aromatic Molecules.* New York: Wileyinterscience, 1970.
24 (a) S. Shaligram, P. P. Wadgaonkar, U. K. Kharul, *J. Mater. Chem. A* 2014, **34**, 13983-13989; (b) W. Sun, J. Z. Wang, H. T. Liu, S. Y. Chang, X. T. Qin, Z. L. Liu, *Mater. Lett.* 2014, **126**, 189-192; (c) D. Tian, R. Y. Chen, J. Xu, Y. W. Li, X. H. Bu, *APL Mater.* 2014, **2**, 124111-124117.
25 (a) D. H. Zhao, T. M. Swager, *Macromolecules* 2005, **38**, 9377-9384; (b) X. H. Zhou, L. Li, H. H. Li, A. Li, T. Yang, W. Huang, *Dalton Trans.* 2013, **42**, 12403-12409.

Graphic Abstract

Rapid and Discriminative Detection of Nitro Aromatic Compounds with High Sensitivity by Two Zinc MOFs Synthesized through Temperature-Modulated Method

Xiu-Yan Wan, Fei-Long Jiang, Cai-Ping Liu, Kang Zhou, Lian Chen*, Yan-Li Gai, Yan Yang and Mao-Chun Hong*

Two 3D fluorescent Zn-MOFs solvothermally synthesized by temperature-modulated method exhibit rapid and discriminative detection of nitro aromatic compounds with high sensitivity.